THE JOURNAL OF PHYSICAL CHEMISTRY A
A JOURNAL OF THE AMERICAN CHEMICAL SOCIETY

pubs.acs.org/JPCA Article

Ability of the Spectroscopic Properties of the P═Se Bond of a Base to Assess Noncovalent Bond Strength

Published as part of The Journal of Physical Chemistry A special issue "Joseph S. Francisco Festschrift".

Mariusz Michalczyk, Wiktor Zierkiewicz, and Steve Scheiner*

Cite This: J. Phys. Chem. A 2025, 129, 545−554 Read Online

ACCESS | Metrics & More | Article Recommendations | Supporting Information

ABSTRACT: The viability of the P═Se bond to serve as a monitor of the strength of a noncovalent bond was tested in the context of the $(CH_3)_3PSe$ molecule. Density functional theory (DFT) computations paired this base with a collection of Lewis acids that spanned hydrogen, halogen, chalcogen, pnicogen, and tetrel bonding interactions and covered a wide range of bond strengths. A very strong linear correlation was observed between the interaction energy and the nuclear magnetic resonance (NMR) $^1J(PSe)$ coupling constant, which could serve as an accurate indicator of bond strength. Also correlating very well with the interaction energy is the stretch of the P═Se bond caused by complexation and the red shift of its stretching frequency. Moderate correlations arise in the chemical shifts of the P and Se nuclei. The σ−hole depth on the Lewis acid is poorly correlated with the energetics, and the same is true for the full electrostatic contribution to the bond energy. Of the various components, it is the polarization energy that correlates most closely with the interaction energy.

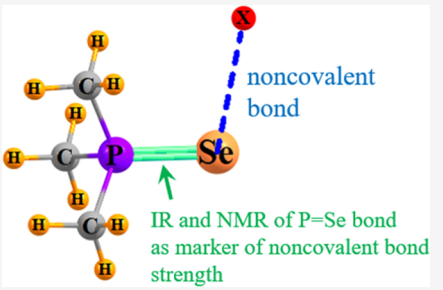

INTRODUCTION

The prevalence and importance of the H-bond (HB) has motivated intense scrutiny over the last century. This noncovalent interaction is a major player in solvation and the structure and function of a wide range of biological systems.[1−5] The HB is partly responsible for the stability of proteins and the mechanism of numerous enzymes. A key means of probing this phenomenon is spectroscopy. One can take as a quantitative measure of the strength of each such bond the degree of shift and intensification that occurs in certain infrared (IR) bands; an alternate metric is associated with the displacement of various nuclear magnetic resonance (NMR) peaks.[6−8] The Badger−Bauer rule relates strength of a given HB to the red shift observed in the covalent A−H stretching frequency of the proton donor,[9−11] NMR spectroscopy offers a similar window, using the downfield shift of the NMR peak of the bridging proton as its key parameter.

The last few decades have reawakened interest in a set of noncovalent bonds that bear a striking resemblance to the HB. In each, the HB proton bridge is replaced by a larger atom, many but not all more electronegative than H. The overall partial charge of the original H occurs instead as a σ−hole, a smaller positive region, surrounded by a negative belt. Depending upon the family of elements from which this replacement atom is drawn, each such σ−hole bond is commonly categorized as a halogen, chalcogen, pnicogen bond, and so forth. But the basics of the HB remain: these noncovalent interactions derive their strength from a mixture of electrostatic, polarization, charge transfer, and dispersion.[12−33] Also in common with the HB, each σ−hole bond is strengthened by electron-withdrawing substituents on the Lewis acid, which intensify this hole. Another factor that enters into the equation is the row of the periodic table. The increasing polarizability and diminishing electronegativity enhance the bond as the bridging atom moves down further in the periodic table, for example, the Cl < Br < I sequence for halogen bonds. First-row atoms, i.e., F, O, N, and C, engage in only weak bonds of this type, if at all, but can be coaxed into measurable interactions by appropriate substituents or adding a charge.[34−40]

Unlike the wide-ranging study of the connection between HB strength and its spectroscopic parameters, such relationships are only now beginning to appear with regard to these σ−hole bonds. As is typical in such emerging studies, the previous work[34,41−56] has been fairly scattered, viewing each particular system individually. The time is ripe for a thorough and systematic treatment of the way in which this bonding affects the spectra as well as an understanding by which these perturbations occur. Such information would permit their unambiguous detection in a given chemical or biological

Received: December 7, 2024
Revised: December 19, 2024
Accepted: December 27, 2024
Published: January 8, 2025

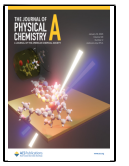

https://doi.org/10.1021/acs.jpca.4c08283
J. Phys. Chem. A 2025, 129, 545−554

system. It would also be especially useful if correlations could be established between certain spectroscopic parameters and the strength or geometry of a given bond, as it has proven to be very informative for HBs over the years.

Work from this laboratory[37,57−61] has examined this question for a number of types of noncovalent bonds. While a certain correlation was observed between bond strength and IR and NMR features of the Lewis acid, these correlations are generally too tenuous to serve as a true quantitative yardstick or only apply to a limited subset of molecules. In contrast to the acid, relationships have been found to be more robust in the context of the Lewis base unit.[46,61,62] As an early example, a theoretical study in 1990,[63] based on prior observations,[64,65] observed a strong linear relationship between the interaction energy and the shift of the C═O stretching frequency of H_2CO when paired with a number of ions.

Later investigations expanded the scope beyond the HB to its related noncovalent sisters. It was found[59] that the spectral and other perturbations caused by these sorts of bonds upon a peptide mimic Lewis base correlated with the bond energy much better than correlations involving the Lewis acid unit. A more recent work[66] observed that the change in the stretching frequency of the C═O bond of a carboxyl group might accurately gauge noncovalent bond strength in certain situations. Further tests of this idea were fruitful,[67] revealing a strong linear relationship between the red shift of the C═O stretching frequency of acetone, as well as the NMR shielding on its C and O atoms, with the strength of a diversity of noncovalent bonds, covering the full range of hydrogen, halogen, chalcogen, pnicogen, and tetrel bonds.

The immediate question arises as to whether it is only the carbonyl C═O for which spectroscopic quantities serve as an accurate measure of intermolecular bond strength. Other work has suggested that the heavier elements involved in the P═Se bond might harbor similar possibilities. An early work[68] suggested the $(CH_3)_3P$═Se molecule as a possible model, focusing on the ^1J(PSe) spin−spin coupling constant. A 2014 paper[69] bore directly on the P═Se bond in the context of PSe···I halogen bonding between triphenyl phosphine and a set of iodoperfluorobenzene derivatives. Direct relationships were observed among halogen bond strength, the ^1J(PSe) coupling constant, and the Se chemical shift, albeit with only three different systems examined. A pair of very recent studies[70,71] have highlighted the usefulness of R_3PSe molecules as potential probes of such bonding via their NMR properties.

The present work is designed to examine this issue in a thorough and systematic manner so as to evaluate the viability of molecules of the R_3PSe type to act as an accurate probe of noncovalent bond strength. Rather than limit the bond type to one particular sort, the quantum calculations cover the full gamut, from H-bonds to halogen, chalcogen, pnicogen, and tetrel bonds. The selection of Lewis acids used to pair with the P═Se base range from quite weak to very strong so as to explore the entire range of bond strength.

METHODS

Geometry optimizations were carried out via the Gaussian 16 (Rev. C.01) package.[72] The density functional theory (DFT) protocol was applied using the M06-2X functional,[73−75] within the framework of the def2-TZVPP basis set. M06-2X has been repeatedly assessed to be one of the most accurate functionals for noncovalent interactions.[76−84] The lack of imaginary harmonic frequencies affirmed the structures as true minima. The Boys−Bernardi counterpoise procedure[85] corrected the basis set superposition error (BSSE). The molecular electrostatic potential (MEP) was analyzed so as to locate and quantify the extrema on the 0.001 au electronic isodensity contour of the isolated monomers, utilizing the MultiWFN software.[86,87] Graphical postprocessing of MEP results was performed using the visual molecular dynamics (VMD) software.[88] QTAIM analysis[89,90] of the electron density topology, by way of the AIMAll program[91] located bond paths and their associated bond critical point parameters. Decomposition of the interaction energy into its various components was accomplished in the framework of the ALMO-EDA scheme via Q-Chem 6[92,93] software.

RESULTS AND DISCUSSION

The molecular electrostatic potential (MEP) surrounding Me_3PSe is illustrated in Figure 1, where the red and blue

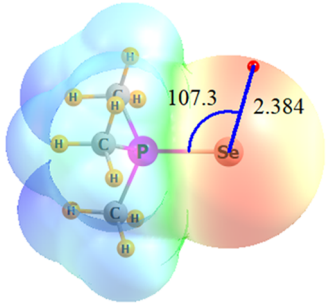

Figure 1. Molecular electrostatic potential (MEP) surrounding Me_3PSe. Blue and red regions refer respectively to positive and negative MEP. A small red ball indicates the position of minimum on 0.001 au isodensity surface, distance in Å, and angle in degs.

areas correspond, respectively, to negative and positive potential. The minimum on the 0.001 au isodensity surface is indicated by the small red ball, which lies 2.384 Å from the Se and which makes an angle of 107.3° with the P═Se bond axis. The value of this MEP minimum is −29.4 kcal/mol. A diverse set of Lewis acids was chosen to pair with Me_3PSe. This list displayed in Scheme 1 results in the formation of hydrogen (HB), halogen (XB), chalcogen (YB), pnicogen (ZB), and tetrel (TB) bonds. The central atom of each acid

Scheme 1. Dimers Examined[a]

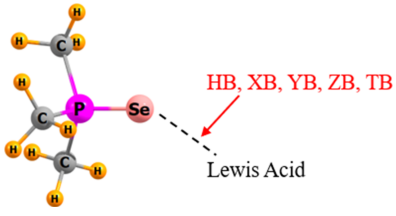

Lewis acids in complexes with Me_3P═Se

HB	XB	YB	ZB	TB
H_2O	C_6H_5Br	C_6H_5SeF	$C_6H_5AsF_2$	$C_6H_5SnF_3$
CH_4	CF_3Br	SF_2	PF_3	GeF_4
HF	FCl	SeF_4	AsF_3	SnF_4
HCl	FI	TeF_2	SbF_3	PbF_4

[a]Abbreviations: HB − hydrogen bond, XB − halogen bond, YB − chalcogen bond, ZB − pnicogen bond, TB − tetrel bond.

https://doi.org/10.1021/acs.jpca.4c08283
J. Phys. Chem. A 2025, 129, 545−554

Table 1. Electrostatic Extrema of Monomers, Interaction Energies, and Geometrical Parameters of Dimers of Lewis Acids with $(CH_3)_3P{=}Se$[a]

dimer	$V_{s,max}$	E_{int}	R (P═Se)	ΔR (P═Se)	R (Se···L)	θ (P═Se···L)
$(CH_3)_3P{=}Se$	−29.4[b]		2.101			
HB						
H_2O	44.3	−8.98	2.118	0.017	2.550	78.3
CH_4	8.7	−1.59	2.103	0.002	3.211	74.9
HF	69.7	−11.73	2.122	0.021	2.313	80.1
HCl	45.2	−8.63	2.119	0.018	2.363	83.8
XB						
C_6H_5Br	9.2	−3.14	2.106	0.005	3.647	83.1
CF_3Br	24.4	−4.62	2.110	0.009	3.467	86.1
FCl	42	−15.33	2.133	0.032	2.666	86.7
FI	60.8	−21.69	2.141	0.040	2.883	92.4
YB						
C_6H_5SeF	28	−12.51	2.125	0.024	3.124	95.0
SF_2	35.9	−8.84	2.119	0.018	3.052	87.6
SeF_4	47.5	−17.42	2.137	0.036	2.998	96.2
TeF_2	56.4	−20.61	2.143	0.042	2.944	93.5
ZB						
$C_6H_5AsF_2$	27.2	−6.75	2.112	0.011	3.534	93.9
PF_3	28.4	−4.18	2.108	0.007	3.486	87.8
AsF_3	40.6	−11.42	2.122	0.021	3.247	96.0
SbF_3	50	−18.61	2.136	0.035	3.156	97.0
TB						
$C_6H_5SnF_3$	26.9	−52.65	2.176	0.075	2.675	98.0
GeF_4	52.6	−33.49	2.152	0.051	2.683	97.1
SnF_4	69.5	−50.88	2.172	0.071	2.701	96.8
PbF_4	70.2	−55.79	2.186	0.085	2.706	96.2

[a]Electrostatic potential and energy in kcal/mol, distances in Å, angles in degrees. [b]$V_{s,min}$

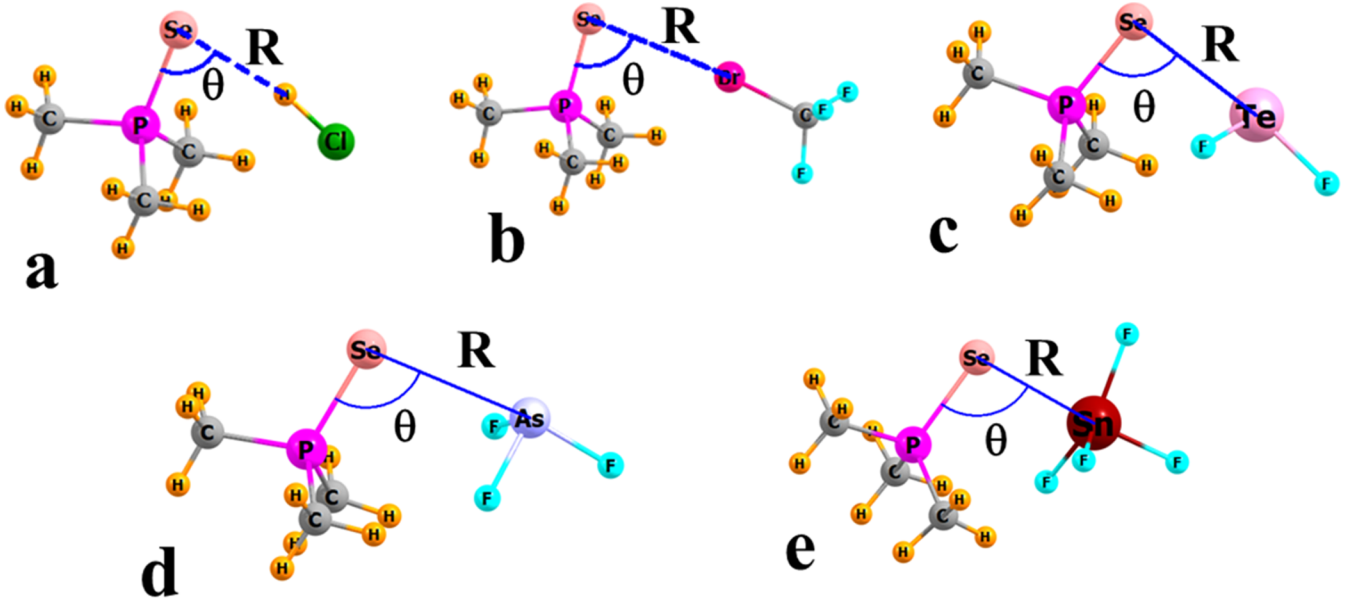

Figure 2. Geometries of representative dyads of Me_3PSe with (a) HCl, (b) CF_3Br, (c) TeF_2, (d) AsF_3, (e) SnF_4.

contains a positive σ−hole, which would naturally align with the negative Se region of the base. The depth of each σ−hole is labeled $V_{s,max}$ and is listed in the first column of Table 1 for each of the Lewis acids. There is a large range of this value, varying between 9 and 70 kcal/mol.

Geometries and IR Spectra. After each Lewis acid molecule was placed in the vicinity of the Se atom of Me_3PSe, the geometry of the dyad was fully optimized, after which a number of properties were elucidated, some of which are reported in Table 1. The optimized structures of some selected dyads are displayed in Figure 2. Just as the σ-hole depths, the interaction energy covers a wide range, varying from less than 1.6 kcal/mol for the very weak CH···Se HB with CH_4 to up to 56 kcal/mol for the tetrel bond with PbF_4. Formation of each noncovalent bond causes the P═Se bond of the base to stretch in the amounts listed in the fourth column of Table 1.

https://doi.org/10.1021/acs.jpca.4c08283
J. Phys. Chem. A 2025, 129, 545−554

The stretch is quite substantial for the more strongly bound dyads, nearly 0.1 Å. Finally, the last two columns contain the most important intermolecular parameters, both the distance between Se and the attacking atom of the Lewis acid L and the angle that this bond makes with the P−Se axis of the base. These angles are fairly small, considerably less than the 107,° which marks the position of the minimum of the MEP. The intermolecular distances cover a wide range, between 2.3 and 3.6 Å. The small radius of the H nucleus leads to the shortest distances in the upper part of Table 1.

Given the substantial stretching of the P═Se bonds upon complexation, it is not surprising to note the ensuing red shift of this bond's stretching frequency. These quantities in Table 2

Table 2. Computed Vibrational Spectral Parameters of Dyads

dimer	ν (P═Se) cm^{-1}	$\Delta\nu$ (P═Se) cm^{-1}	I (P═Se) km/mol	I_{comp}/I_{mon}
$(CH_3)_3$ P═Se	461		25	
HB				
H_2O	452	−9	29	1.16
CH_4	460	−1	24	0.98
HF	449	−12	26	1.04
HCl	450	−11	25	1.01
XB				
C_6H_5Br	457	−4	23	0.92
CF_3Br	456	−5	25	1.01
FCl	442	−19	46	1.83
FI	438	−23	41	1.64
YB				
C_6H_5SeF	446	−15	30	1.21
SF_2	450	−11	27	1.08
SeF_4	440	−21	25	1.00
TeF_2	436	−25	32	1.27
ZB				
$C_6H_5AsF_2$	455	−6	25	1.02
PF_3	456	−5	27	1.07
AsF_3	449	−12	31	1.25
SbF_3	441	−20	35	1.38
TB				
$C_6H_5SnF_3$	427	−34	19	0.76
GeF_4	435	−26	19	0.75
SnF_4	424	−37	23	0.93
PbF_4	416	−45	28	1.14

vary from 1 cm^{-1} for the very weakly bound CH_4 all the way up to 45 cm^{-1} in the case of the tightly bound tetrel bond with PbF_4. The last two columns of Table 2 report the calculated intensity of this band and the ratio between that in the complex and the intensity of the monomer. In most cases, this intensity is magnified, but there are also cases where it is diminished, particularly for the tetrel bonds at the bottom of the Table.

The stretch of the P═Se bond and the red shift of its stretching frequency serve as excellent markers of the strength of the bond. Figure 3 shows that there is a strong linear correlation between each of these quantities and E_{int}. The correlation coefficients R^2 for ΔR and $\Delta\nu$ are equal to 0.97 and 0.92, respectively. The slope of the $\Delta\nu$ line is such that each 10 cm^{-1} decrement of the stretching frequency translates to some 13 kcal/mol rise in the interaction energy.

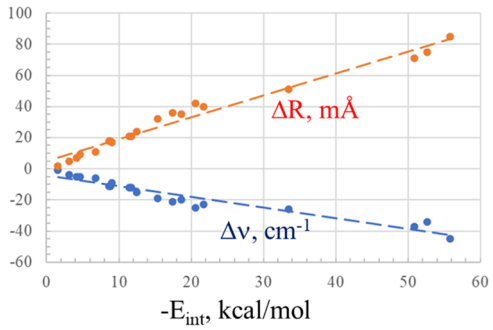

Figure 3. Relation between interaction energy and stretch of intermolecular distance and red shift of P═Se stretching frequency. The equations of best fit are $\Delta R = 1.41(-E_{int}) + 5.0$ and $\Delta\nu = -0.68(-E_{int}) - 4.4$, with respective correlation coefficients equal to 0.97 and 0.92.

NMR Properties. In addition to IR data, NMR spectroscopic parameters have proven their worth for assessing H-bond strengths. Some of the NMR properties of electron donor Me_3PSe are reported in Table 3. The first column lists the chemical shielding σ of the P atom, followed in the next column by the chemical shift δ relative to the H_3PO_4 standard. The following column calculates the change in this shift induced in the base by the interaction with the indicated Lewis acid. The positive quantities for $\Delta\delta$(P) reflect a reduced shielding and are as large as 11 ppm. The next three columns collect analogous data for the Se nucleus, which has δ values between −276 and +137 ppm. Due in large measure to its direct interaction with the acid, the perturbations of δ for the Se nucleus are much larger than for P, some as large as 400 ppm. Again, the positive values of these changes in δ indicate deshielding caused by the bonding. The final two columns of Table 3 display the coupling constant between the P and Se nuclei, which is −636 Hz for the unperturbed base. The noncovalent bonding with the various acids causes this quantity to become less negative and by a substantial amount. The largest ΔJ of 257 Hz constitutes a drop in magnitude by some 40%.

The NMR spectroscopic perturbations arising from complexation correlate with the interaction energy, albeit not as closely as does the red shift of the P═Se stretch. The relationships are delineated in Figure 4, where the orange curve corresponds to the change in the P−Se coupling constant. The blue and green points refer to the change in the chemical shifts of Se and P, respectively (with the latter multiplied by a factor of 10 to fit into the same diagram as the others). The Se shielding changes are rather scattered, with a correlation coefficient of only 0.58. The corresponding P shifts are a bit more focused with $R^2 = 0.64$. But these correlations are probably not strong enough that these changes can be used as an accurate barometer of bond strength. The coupling constant, however, does correlate very well with E_{int}. Its correlation coefficient is 0.96, allowing it to provide a very strong connection between NMR spectroscopy and the bond strength.

There is experimental verification of some of the trends observed here. Earlier studies[69] of PSe···I halogen bonding found that strengthening of the noncovalent bond diminishes the magnitude of J(PSe), as was noted here in Table 3. Also consistent with the computational data is the increase in the chemical shift of both P and Se. Another aspect of the

https://doi.org/10.1021/acs.jpca.4c08283
J. Phys. Chem. A 2025, 129, 545−554

Table 3. Computed NMR Parameters of Dimers

dimer	σ(P)[b]	δ(P)[c]	$\Delta\delta$(P)[d]	σ(Se)	δ(Se)	$\Delta\delta$(Se)	J_{PSe}	ΔJ_{PSe}
$(CH_3)_3P{=}Se$[a]	250.8	40.2		2135.9	−273.0		−636	
HB								
H_2O	245.3	45.8	5.6	2129.6	−266.7	6.3	−582	54
CH_4	250.3	40.7	0.5	2138.4	−275.5	−2.5	−630	7
HF	244.2	46.9	6.6	2123.0	−260.1	13.0	−559	78
HCl	246.1	45.0	4.7	2082.8	−219.9	53.2	−571	66
XB								
C_6H_5Br	249.7	41.4	1.2	2121.3	−258.4	14.6	−622	15
CF_3Br	249.0	42.1	1.9	2106.0	−243.1	30.0	−608	29
FCl	241.9	49.2	9.0	1972.8	−109.9	163.1	−516	121
FI	241.7	49.4	9.2	2075.1	−212.2	60.9	−500	137
YB								
C_6H_5SeF	246.7	44.4	4.2	2016.3	−153.4	119.7	−572	65
SF_2	245.8	45.3	5.1	1998.3	−135.4	137.7	−577	59
SeF_4	244.0	47.1	6.8	1907.4	−44.5	228.5	−526	110
TeF_2	242.3	48.8	8.6	1885.1	−22.2	250.8	−510	126
ZB								
$C_6H_5AsF_2$	247.6	43.4	3.2	2099.6	−236.7	36.4	−604	32
PF_3	250.0	41.1	0.9	2084.5	−221.6	51.4	−610	27
AsF_3	246.1	45.0	4.8	2036.0	−173.1	99.9	−570	66
SbF_3	243.8	47.2	7.0	1972.2	−109.3	163.7	−529	107
TB								
$C_6H_5SnF_3$	240.7	50.4	10.1	1947.8	−84.9	188.1	−407	229
GeF_4	244.6	46.4	6.2	1957.8	−94.9	178.1	−470	166
SnF_4	241.9	49.1	8.9	1945.7	−82.8	190.2	−411	225
PbF_4	239.7	51.4	11.2	1725.5	137.4	410.5	−379	257

Shielding (σ) and shift (δ) in ppm, coupling constant (J) in Hz [a]data for the $(CH_3)_3P{=}Se$ monomer, [b]σ - shielding constant, [c]δ - chemical shift calculated from the formula:$\delta = \sigma$(reference) − $\sigma\sigma$(reference) for ^{31}P is 291.1 ppm (reference compound H_3PO_4), while for ^{77}Se the σ(reference) is 1862.9 ppm (reference $Se(CH_3)_2$). [d]$\Delta\delta = \delta$(complex) − δ(monomer)

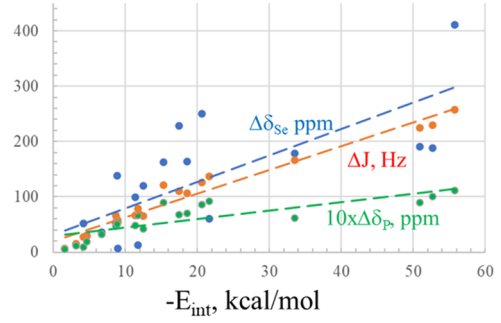

Figure 4. Relation between interaction energy and NMR parameters. The equations of best fit are $\Delta\delta_{Se} = 4.78(-E_{int}) + 31.4$, $\Delta J = 4.29(-E_{int}) + 19.6$, and $10 \times \Delta\delta_P = 1.51(-E_{int}) + 29.9$ with respective correlation coefficients equal to 0.58, 0.96, and 0.64.

computations supported by the X-ray data is the stretch of the P═Se bond caused by complexation. With regard to absolute values, the J(PSe) computed here for Me_3PSe of 636 Hz is quite similar to a measurement of 635 Hz in solution.[70] R_3PSe was directly involved in Se···I and Se···Br halogen bonding with aromatic Lewis acids.[71] This bonding led to a decrease in J(PSe) and a deshielding of the Se nucleus, consistent with the calculations described above.

Electron Density. The topology of the electron density offers other sorts of insights into the nature and strength of bonding. Whether the density is elucidated directly from diffraction data or calculated quantum mechanically, one can apply the Atoms in Molecules (AIM) methodology to elucidate bond paths connecting atoms to one another. The numerical values of certain properties at the bond critical point joining Se to the Lewis acid atom L are thought to accurately assess the strength of each bond. The most commonly used parameters for this purpose are listed in Table 4, where ρ refers to the density at the bond critical point, and $\nabla^2\rho$ its Laplacian. V and G correspond to the potential and kinetic energy densities, respectively, and their ratios are listed in the final column. The relationship between some of these AIM properties and the interaction energy can be seen in Figure 5 to be nearly linear. The correlation coefficients for such a linear relationship are equal to 0.83 for ρ but only 0.31 for $\nabla^2\rho$, so the latter quantity is ruled out as a useful measure of bond strength. The best correlation is achieved for the potential energy density V, for which $R^2 = 0.89$.

Some previous papers have taken the value of V as a proportional measure of the noncovalent bond energy.[94−96] For example, the equation $E_{int} = 0.5 \times V$ has been applied to H-bonds. When both are expressed in the same units, the slope of the V curve in Figure 5 for the Se···L bond translates to a much steeper relationship of $E_{int} = 1.8 \times V$. In other words, each 0.01 au (equal to 6.3 kcal/mol) increment in the magnitude of V corresponds to a 10 kcal/mol rise in the interaction energy.

In connection with the AIM analysis, the full molecular diagrams of each dyad are displayed in Figure S1. It may be noted there that in addition to the noncovalent bond of interest to the Se on the base, the AIM protocol draws a bond path in many cases to a methyl H atom. Although these bonds are weak as judged by their bond critical point densities, their presence would tend to deteriorate the correlation between E_{int}

https://doi.org/10.1021/acs.jpca.4c08283
J. Phys. Chem. A 2025, 129, 545−554

Table 4. QTAIM Parameters for Dyads, All in au of Electron Density (electron/Bohr^3) or Energy (Hartree)

dimer	ρ	$\nabla^2\rho$	V	G	$-G/V$
HB					
H_2O	0.017	0.039	−0.009	0.010	1.11
CH_4	0.006	0.014	−0.002	0.003	1.50
HF	0.027	0.037	−0.017	0.013	0.76
HCl	0.027	0.036	−0.015	0.012	0.80
XB					
C_6H_5Br	0.009	0.024	−0.004	0.005	1.25
CF_3Br	0.012	0.031	−0.006	0.007	1.17
FCl	0.048	0.069	−0.031	0.024	0.77
FI	0.043	0.051	−0.028	0.020	0.71
YB					
C_6H_5SeF	0.023	0.042	−0.012	0.012	1.00
SF_2	0.024	0.046	−0.013	0.012	0.92
SeF_4	0.034	0.038	−0.017	0.013	0.76
TeF_2	0.038	0.041	−0.024	0.017	0.71
ZB					
$C_6H_5AsF_2$	0.012	0.024	−0.005	0.006	1.20
PF_3	0.012	0.023	−0.005	0.006	1.20
AsF_3	0.020	0.030	−0.010	0.008	0.80
SbF_3	0.027	0.029	−0.014	0.011	0.79
TB					
$C_6H_5SnF_3$	0.056	0.065	−0.045	0.031	0.69
GeF_4	0.049	0.008	−0.037	0.020	0.54
SnF_4	0.054	0.057	−0.042	0.028	0.67
PbF_4	0.061	0.059	−0.046	0.030	0.65

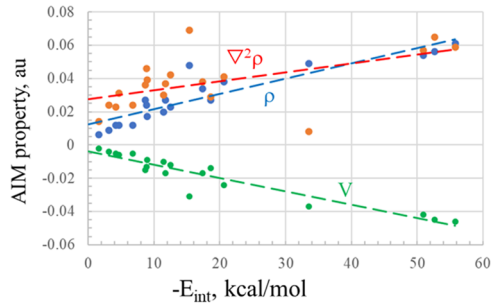

Figure 5. Relation between interaction energy and AIM properties of Se···L bond critical point. The equations of best fit are ρ = 0.0009($-E_{int}$) + 0.013, $\nabla^2\rho$ = 0.0005($-E_{int}$) + 0.028, and V = 0.0008($-E_{int}$) − 0.0004 with respective correlation coefficients equal to 0.83, 0.31, and 0.89.

that represents an aggregate of any bonding interactions and the primary noncovalent bond parameters.

Energy Decomposition. One can extract fundamental insights into the nature of a given noncovalent bond by partitioning the total interaction energy into its physically meaningful components. The total interaction energy of each dyad was separated into its components by ALMO-EDA decomposition, which provides electrostatic (ELEC), dispersion (DISP), polarization (POL), and charge transfer (CT) as separate attractive elements, all countered by Pauli repulsion. The magnitudes of these components are listed in Table 5, supplemented by their percentage contribution to the total attractive energy. The first feature that arises from the inspection of these quantities is the major contribution arising from electrostatics. ELEC accounts for between half and 2:3 of the total attractive force. Dispersion and charge transfer are comparable to one another, with their relative contributions being variable across the spectrum of systems. In general, CT is the larger of these two for the tetrel bonds, while the reverse is true for the pnicogen bonds. The polarization energy is typically the smallest component but does account for a larger share of the tetrel bonds.

Given this variability, it is logical that none of these quantities in and of themselves serve as a suitable barometer of the full interaction energy. The polarization tracks the best, with R^2 = 0.91. DISP is worse, with a correlation coefficient of only 0.59. Given its fairly large share of the total, the performance of ELEC is disappointing in this respect, with a correlation coefficient of 0.22, with CT even worse at 0.18. One component of the electrostatic energy is associated with the Coulombic attraction between the negatively charged Se atom of the base and the positive σ−hole of each Lewis acid. Since the correlation between E_{int} and the entire ES component is poor, it is sensible that the correlation with simply V_{max} is equally weak, only 0.31.

Comparison with Carbonyl Group. The double-bonded P═Se group of Me_3PSe has certain similarities with the C═O carbonyl of Me_2CO, so a direct comparison offers the opportunity to learn more about each from a fundamental perspective. The similarly methylated Me_2CO was studied recently by an identical theoretical approach[67] which facilitates such comparisons. The interaction energies involving Se as the electron donor tend to be somewhat larger. The halogen bond to IF, for example, rises from 13.3 kcal/mol for Me_2CO up to 21.7 for Me_3PSe. The tetrel bonds are particularly enhanced: for example, the bonds to PbF_4 are 31.1 and 55.8 kcal/mol, respectively. The stronger interactions with the Se arise despite the V_{min} on this atom being less negative at −29.4 kcal/mol, as compared to −37.2 on the O center of Me_2CO. As a second distinction, the P═Se bond is much more "stretchable" than C═O. The changes in the former bond length arising from the interactions with each Lewis acid are considerably larger. Another distinction related to the geometries is that the θ(P═Se···L) angles are much more acute than those for θ(C═O···L), which hover around 120°.

With regard to spectroscopic data, the red shifts of the P═Se stretching frequency are considerably smaller than those of C═O. For example, the largest such shift observed here for P═Se is −45 cm^{-1}, as compared to −98 cm^{-1} for the carbonyl. Some of this contrast may be due to the heavier P and Se atoms. NMR chemical shifts on the P atom caused by complexation are in the same direction as the C of C═O, with both experiencing a reduced shielding. The magnitudes are quite a bit smaller for P than C, however, by a factor of 3 in some cases. It is the atom directly involved in the interaction where the two types of systems most strongly diverge. Whereas the shielding on the carbonyl O atom is increased by the various noncovalent bonds, that on the Se drops. There is a slightly lesser dependence of the Se···L interaction energies on the electrostatic component, as compared to carbonyl, which is compensated by a larger charge transfer element.

CONCLUSIONS

Table 6 summarizes the ability of each quantity considered above to predict the interaction energy. The table is organized with a diminishing correlation coefficient from top to bottom. As may be seen, the stretch of the P═Se bond length tracks the best with bond energy, with a correlation coefficient of 0.97. Also, an excellent predictor is the NMR P−Se coupling constant, with R^2 = 0.96. Related to the P═Se bond stretch is

https://doi.org/10.1021/acs.jpca.4c08283
J. Phys. Chem. A 2025, 129, 545−554

Table 5. ALMO-EDA Decomposition of Interaction Energies (kcal/mol)[a]

dimer	E_{int}	ELEC	%	PAULI	DISP	%	POL	%	CT	%	total
HB											
H_2O	−8.98	−19.24	67	19.56	−4.78	17	−1.89	7	−2.63	9	−8.98
CH_4	−1.59	−4.64	55	6.91	−2.84	33	−0.41	5	−0.60	7	−1.59
HF	−11.73	−22.01	64	22.77	−4.62	13	−2.93	8	−4.94	14	−11.73
HCl	−8.63	−18.22	57	23.60	−5.00	16	−2.38	7	−6.62	21	−8.63
XB											
C_6H_5Br	−3.14	−8.75	58	11.96	−4.08	27	−0.68	5	−1.56	10	−3.11
CF_3Br	−4.62	−11.49	60	14.69	−4.35	23	−0.99	5	−2.46	13	−4.60
FCl	−15.33	−31.94	44	57.77	−8.13	11	−4.42	6	−28.58	39	−15.30
FI	−21.69	−41.49	48	64.33	−11.16	13	−8.30	10	−25.06	29	−21.68
YB											
C_6H_5SeF	−12.51	−28.46	53	40.99	−12.28	23	−3.99	7	−8.78	16	−12.51
SF_2	−8.84	−22.37	55	32.01	−7.43	18	−2.22	5	−8.80	22	−8.82
SeF_4	−17.42	−38.76	56	51.76	−10.14	15	−5.69	8	−14.60	21	−17.43
TeF_2	−20.61	−41.10	50	60.95	−11.66	14	−8.76	11	−20.03	25	−20.60
ZB											
$C_6H_5AsF_2$	−6.75	−17.69	62	21.66	−6.87	24	−1.44	5	−2.45	9	−6.78
PF_3	−4.18	−11.92	58	16.54	−5.22	25	−1.14	5	−2.46	12	−4.19
AsF_3	−11.42	−26.50	61	31.69	−7.93	18	−3.01	7	−5.65	13	−11.40
SbF_3	−18.61	−32.02	54	41.00	−10.94	18	−6.59	11	−10.01	17	−18.56
TB											
$C_6H_5SnF_3$	−52.65	−77.47	52	95.21	−13.20	9	−28.08	19	−29.11	20	−52.64
GeF_4	−33.49	−64.46	56	82.11	−12.67	11	−17.53	15	−20.97	18	−33.51
SnF_4	−50.88	−71.55	52	86.45	−12.71	9	−25.32	18	−27.75	20	−50.88
PbF_4	−55.79	−80.26	50	103.38	−13.85	9	−24.43	15	−40.67	26	−55.83

[a]Electrostatic term (ELEC), Pauli repulsion (PAULI), dispersion (DISP), polarization (POL), charge transfer (CT). Percentage contributions are listed as fraction of sum of attractive elements.

Table 6. Correlation Coefficients Relating Interaction Energy with Indicated Property for a Set of 20 Dimers

property	R^2
ΔR (P═Se)	0.97
ΔJ_{PSe}	0.96
$\Delta\nu$ (P═Se)	0.92
%POL	0.91
V	0.89
ρ	0.82
$\Delta\delta$(P)	0.64
%DISP	0.59
$\Delta\delta$(Se)	0.58
−G/V	0.49
∠(P═Se···L)	0.40
$\nabla^2\rho$	0.31
$V_{s,max}$	0.31
%ELEC	0.22
R (Se···L)	0.21
%CT	0.18
I_{comp}/I_{mon}	0.03

the red shift of its vibrational frequency, where the correlation coefficient is still excellent at 0.92. Given the small contribution of the polarization energy to the total interaction, it is surprising to note that it is a fairly good match with the latter, with R^2 = 0.91. Of the various AIM quantities, it is the potential energy density that best matches the interaction energy, with a correlation coefficient of 0.89, followed by the density for which R^2 = 0.82.

There is marked deterioration as one progresses down the remainder of Table 6, with all correlation coefficients appreciably below 0.7. Only modest correlations are observed for the NMR shifts of both the P and Se nuclei. Given the heavy reliance of the interaction energy upon the electrostatic component, the weak correlations of both ELEC and $V_{s,max}$ are notable. Whereas the red shift of the P═Se stretching frequency correlates quite well with the interaction energy, the opposite is true for its intensity change.

The IR correlations for the P═Se systems are not quite as good as those for the carbonyl. The correlation coefficient for the C═O red shift with the interaction energy is 0.96, slightly better than the 0.92 for the P═Se analogue. The chemical shifts of the related atoms suffer more from the switch from carbonyl. The correlation coefficient of both the C and the O shielding was 0.96, which is much poorer for P and Se at 0.64 and 0.58, respectively. What is identified here as the best parameter by which to gauge the strength of the interaction with the P═Se group is the NMR coupling constant, with a correlation coefficient of 0.96. (Correlations between all pairs of properties are displayed in Figure S2.)

It should finally be underscored that Badger-Bauer and related relations that have found so much use over the years can perhaps attribute much of their success to the narrowness of their applications. They are limited to H-bonds and usually applied to a set of closely related systems that cover only a narrow range of energetics. In contrast, the systems considered here are quite diverse, varying from H-bonds to halogen, chalcogen, pnicogen, and tetrel bonds, each with somewhat different origins. Also, the bond strengths cover a wide spectrum, from less than 2 to nearly 60 kcal/mol. The nearly perfect linear relation between the J(PSe) coupling constant and the interaction energy over this entire set of systems can thus be considered quite remarkable. The same can be said of

https://doi.org/10.1021/acs.jpca.4c08283
J. Phys. Chem. A 2025, 129, 545−554

the red shift of the P═Se stretching frequency, even if the correlation coefficient is not quite as close to unity. Even the chemical shifts of the P and Se atoms bear a reasonable correlation with the interaction energy, so they might be used in a semiquantitative manner, if the other data are not amenable to measurement.

■ ASSOCIATED CONTENT

Supporting Information

The Supporting Information is available free of charge at https://pubs.acs.org/doi/10.1021/acs.jpca.4c08283.

AIM diagrams; correlations; and Cartesian coordinates of complexes (PDF)

■ AUTHOR INFORMATION

Corresponding Author

Steve Scheiner − *Department of Chemistry and Biochemistry, Utah State University, Logan, Utah 84322-0300, United States;* orcid.org/0000-0003-0793-0369; Email: steve.scheiner@usu.edu

Authors

Mariusz Michalczyk − *Faculty of Chemistry, Wrocław University of Science and Technology, Wrocław 50-370, Poland;* orcid.org/0000-0002-6495-6963

Wiktor Zierkiewicz − *Faculty of Chemistry, Wrocław University of Science and Technology, Wrocław 50-370, Poland;* orcid.org/0000-0002-4038-5959

Complete contact information is available at: https://pubs.acs.org/10.1021/acs.jpca.4c08283

Notes

The authors declare no competing financial interest.

■ ACKNOWLEDGMENTS

The authors gratefully acknowledge Polish high-performance computing infrastructure PLGrid (HPC Centers: ACK Cyfronet AGH) for providing computer facilities and support within computational grant no. PLG/2023/016853, Wrocław Center for Networking and Supercomputing (WCSS). This material is also based upon work supported by the U.S. National Science Foundation under Grant No. 1954310 to S.S. This work was financed in part by a statutory activity subsidy from the Polish Ministry of Science and Higher Education for the Faculty of Chemistry of Wroclaw University of Science and Technology.

■ REFERENCES

(1) Hadzi, D.; Bratos, S. *The Hydrogen Bond. Recent Developments in Theory and Experiments*; Schuster, P.; Zundel, G.; Sandorfy, C., Eds.; North-Holland Publishing Co.: Amsterdam, 1976; Vol. 2, pp 565−611.

(2) Scheiner, S. Comparison of proton transfers in heterodimers and homodimers of NH_3 and OH_2. *J. Chem. Phys.* **1982**, *77*, 4039−4050.

(3) Vener, M. V.; Scheiner, S. Hydrogen bonding and proton transfer in the ground and lowest excited singlet states of o-hydroxyacetophenone. *J. Phys. Chem. A* **1995**, *99*, 642−649.

(4) Gilli, G.; Gilli, P. *The Nature of the Hydrogen Bond*; Oxford University Press: Oxford, UK, 2009.

(5) Scheiner, S. *Hydrogen Bonding: A Theoretical Perspective*; Oxford University Press: New York, 1997.

(6) Rivera-Rivera, L. A.; McElmurry, B. A.; Scott, K. W.; Lucchese, R. R.; Bevan, J. W. The Badger−Bauer Rule Revisited: Correlation of Proper Blue Frequency Shifts in the OC Hydrogen Acceptor with Morphed Hydrogen Bond Dissociation Energies in OC−HX (X = F, Cl, Br, I, CN, CCH). *J. Phys. Chem. A* **2013**, *117*, 8477−8483.

(7) Cook, J. L.; Hunter, C. A.; Low, C. M. R.; Perez-Velasco, A.; Vinter, J. G. Solvent effects on hydrogen bonding. *Angew. Chem., Int. Ed.* **2007**, *46*, 3706−3708.

(8) Du, L.; Mackeprang, K.; Kjaergaard, H. G. Fundamental and overtone vibrational spectroscopy, enthalpy of hydrogen bond formation and equilibrium constant determination of the methanol-dimethylamine complex. *Phys. Chem. Chem. Phys.* **2013**, *15*, 10194−10206.

(9) Schuster, P.; Zundel, G.; Sandorfy, C. *The Hydrogen Bond. Recent Developments in Theory and Experiments.*; North-Holland Publishing Co.: Amsterdam, 1976.

(10) Boyer, M. A.; Marsalek, O.; Heindel, J. P.; Markland, T. E.; McCoy, A. B.; Xantheas, S. S. Beyond Badger's Rule: The Origins and Generality of the Structure−Spectra Relationship of Aqueous Hydrogen Bonds. *J. Phys. Chem. Lett.* **2019**, *10*, 918−924.

(11) Thatcher, R. J.; Johnson, D. G.; Slattery, J. M.; Douthwaite, R. E. Structure of Amido Pyridinium Betaines: Persistent Intermolecular C−H···N Hydrogen Bonding in Solution. *Chem. - Eur. J.* **2016**, *22*, 3414−3421.

(12) Del Bene, J. E.; Alkorta, I.; Elguero, J. Exploring N···C tetrel and O···S chalcogen bonds in HN(CH)SX:OCS systems, for X = F, NC, Cl, CN, CCH, and H. *Chem. Phys. Lett.* **2019**, *730*, 466−471.

(13) Gougoula, E.; Medcraft, C.; Alkorta, I.; Walker, N. R.; Legon, A. C. A chalcogen-bonded complex $H_3N{\cdots}S{=}C{=}S$ formed by ammonia and carbon disulfide characterised by chirped-pulse, broadband microwave spectroscopy. *J. Chem. Phys.* **2019**, *150*, No. 084307.

(14) Alkorta, I.; Legon, A. An Ab Initio Investigation of the Geometries and Binding Strengths of Tetrel-, Pnictogen-, and Chalcogen-Bonded Complexes of CO_2, N_2O, and CS_2 with Simple Lewis Bases: Some Generalizations. *Molecules* **2018**, *23*, No. 2250.

(15) Grabowski, S. J. Pnicogen and tetrel bonds—tetrahedral Lewis acid centres. *Struct. Chem.* **2019**, *30*, 1141−1152.

(16) Grabowski, S. Tetrel Bonds with π-Electrons Acting as Lewis Bases—Theoretical Results and Experimental Evidences. *Molecules* **2018**, *23*, No. 1183.

(17) Alkorta, I.; Elguero, J.; Grabowski, S. J. Pnicogen and hydrogen bonds: complexes between PH_3X^+ and PH_2X systems. *Phys. Chem. Chem. Phys.* **2015**, *17*, 3261−3272.

(18) Scheiner, S. Participation of transition metal atoms in noncovalent bonds. *Phys. Chem. Chem. Phys.* **2024**, *26*, 27382−27394.

(19) Franconetti, A.; Frontera, A. Theoretical and Crystallographic Study of Lead(IV) Tetrel Bonding Interactions. *Chem. - Eur. J.* **2019**, *25*, 6007−6013.

(20) Frontera, A.; Bauzá, A. S···Sn Tetrel Bonds in the Activation of Peroxisome Proliferator-Activated Receptors (PPARs) by Organotin Molecules. *Chem. - Eur. J.* **2018**, *24*, 16582−16587.

(21) Murray, J. S.; Politzer, P. σ-Holes and Si···N intramolecular interactions. *J. Mol. Model.* **2019**, *25*, No. 101.

(22) Clark, T.; Murray, J. S.; Politzer, P. A perspective on quantum mechanics and chemical concepts in describing noncovalent interactions. *Phys. Chem. Chem. Phys.* **2018**, *20*, 30076−30082.

(23) Riley, K. E.; Tran, K.-A. Strength, character, and directionality of halogen bonds involving cationic halogen bond donors. *Faraday Discuss.* **2017**, *203*, 47−60.

(24) Riley, K. E.; Vazquez, M.; Umemura, C.; Miller, C.; Tran, K.-A. Exploring the (Very Flat) Potential Energy Landscape of R−Br···π Interactions with Accurate CCSD(T) and SAPT Techniques. *Chem. - Eur. J.* **2016**, *22*, 17690−17695.

(25) Zierkiewicz, W.; Michalczyk, M.; Wysokiński, R.; Scheiner, S. Dual Geometry Schemes in Tetrel Bonds: Complexes between TF_4 (T = Si, Ge, Sn) and Pyridine Derivatives. *Molecules* **2019**, *24*, No. 376.

(26) Zierkiewicz, W.; Fanfrlík, J.; Michalczyk, M.; Michalska, D.; Hobza, P. S···N chalcogen bonded complexes of carbon disulfide with diazines. Theoretical study. *Chem. Phys.* **2018**, *500*, 37−44.

(27) Dong, W.; Niu, B.; Liu, S.; Cheng, J.; Liu, S.; Li, Q. Comparison of σ-/π-Hole Tetrel Bonds between TH_3F/F_2TO and H_2CX (X═O, S, Se). *ChemPhysChem* **2019**, *20*, 627−635.
(28) Dong, W.; Wang, Y.; Cheng, J.; Yang, X.; Li, Q. Competition between σ-hole pnicogen bond and π-hole tetrel bond in complexes of CF_2═$CFZH_2$ (Z = P, As, and Sb). *Mol. Phys.* **2019**, *117*, 251−259.
(29) Stasyuk, O. A.; Sedlak, R.; Guerra, C. F.; Hobza, P. Comparison of the DFT-SAPT and Canonical EDA Schemes for the Energy Decomposition of Various Types of Noncovalent Interactions. *J. Chem. Theory Comput.* **2018**, *14*, 3440−3450.
(30) Sedlak, R.; Eyrilmez, S. M.; Hobza, P.; Nachtigallova, D. The role of the s-holes in stability of non-bonded chalcogenide···benzene interactions: the ground and excited states. *Phys. Chem. Chem. Phys.* **2018**, *20*, 299−306.
(31) Esrafili, M. D.; Mousavian, P. Strong Tetrel Bonds: Theoretical Aspects and Experimental Evidence. *Molecules* **2018**, *23*, No. 2642.
(32) Scheiner, S.; Adhikari, U. Abilities of different electron donors (D) to engage in a P···D noncovalent interaction. *J. Phys. Chem. A* **2011**, *115*, 11101−11110.
(33) Scheiner, S. Modulating the Competition between Different Atoms to Form Halogen Bonds. *J. Phys. Chem. A* **2024**, *128*, 9939−9946.
(34) Bene, J. E. D.; Alkorta, I.; Elguero, J. Anionic complexes of F^- and Cl^- with substituted methanes: Hydrogen, halogen, and tetrel bonds. *Chem. Phys. Lett.* **2016**, *655*−*656*, 115−119.
(35) Scheiner, S. Can two trivalent N atoms engage in a direct N···N noncovalent interaction? *Chem. Phys. Lett.* **2011**, *514*, 32−35.
(36) Southern, S. A.; Bryce, D. L. NMR Investigations of Noncovalent Carbon Tetrel Bonds. Computational Assessment and Initial Experimental Observation. *J. Phys. Chem. A* **2015**, *119*, 11891−11899.
(37) Scheiner, S. Comparison of CH···O, SH···O, Chalcogen, and Tetrel Bonds Formed by Neutral and Cationic Sulfur-Containing Compounds. *J. Phys. Chem. A* **2015**, *119*, 9189−9199.
(38) Nziko, V. D. P. N.; Scheiner, S. Comparison of p-hole tetrel bonding with s-hole halogen bonds in complexes of XCN (X = F, Cl, Br, I) and NH_3. *Phys. Chem. Chem. Phys.* **2016**, *18*, 3581−3590.
(39) Liu, M.; Li, Q.; Scheiner, S. Comparison of tetrel bonds in neutral and protonated complexes of pyridineTF_3 and furanTF_3 (T = C, Si, and Ge) with NH_3. *Phys. Chem. Chem. Phys.* **2017**, *19*, 5550−5559.
(40) Scheiner, S. Systematic Elucidation of Factors That Influence the Strength of Tetrel Bonds. *J. Phys. Chem. A* **2017**, *121*, 5561−5568.
(41) Alkorta, I.; Rozas, S.; Elguero, J. Charge-transfer complexes between dihalogen compounds and electron donors. *J. Phys. Chem. A* **1998**, *102*, 9278−9285.
(42) Zhou, Z.-J.; Liu, H.-L.; Huang, X.-R.; Li, Q.-Z.; Sun, C.-C. Effect of substitution and cooperativity on the Cl−F blue shift in single-electron halogen-bonded H3C ··· ClF complex. *Mol. Phys.* **2010**, *108*, 2021−2026.
(43) Wang, W.; Zhang, Y.; Ji, B.; Tian, A. On the correlation between bond-length change and vibrational frequency shift in halogen-bonded complexes. *J. Chem. Phys.* **2011**, *134*, No. 224303.
(44) Ford, T. A. An ab initio study of some halogen-bonded complexes containing cyclic ethers. *Mol. Phys.* **2021**, *119*, No. e1919326.
(45) Bene, J. E. D.; Alkorta, I.; Elguero, J. Properties of cationic pnicogen-bonded complexes $F_{4-n}H_nP^+$:N-base with H−P···N linear and n = 1−4. *Mol. Phys.* **2016**, *114*, 102−117.
(46) Ellington, T. L.; Reves, P. L.; Simms, B. L.; Wilson, J. L.; Watkins, D. L.; Tschumper, G. S.; Hammer, N. I. Quantifying the Effects of Halogen Bonding by Haloaromatic Donors on the Acceptor Pyrimidine. *ChemPhysChem* **2017**, *18*, 1267−1273.
(47) Esrafili, M. D.; Vakili, M. The effect of hydrogen-bonding cooperativity on the strength and properties of σ-hole interactions: an ab initio study. *Mol. Phys.* **2017**, *115*, 913−924.
(48) Gholipour, A.; Farhadi, S.; Neyband, R. S. Theoretical investigation of the nature and strength of simultaneous interactions of π−π stacking and halogen bond including NMR, SAPT, AIM and NBO analysis. *Struct. Chem.* **2016**, *27*, 1543−1551.
(49) Cormanich, R. A.; Rittner, R.; O'Hagan, D.; Bühl, M. Inter- and intramolecular CF···C═O interactions on aliphatic and cyclohexane carbonyl derivatives. *J. Comput. Chem.* **2016**, *37*, 25−33.
(50) Viger-Gravel, J.; Leclerc, S.; Korobkov, I.; Bryce, D. L. Correlation between ^{13}C chemical shifts and the halogen bonding environment in a series of solid para-diiodotetrafluorobenzene complexes. *CrystEngComm* **2013**, *15*, 3168−3177.
(51) Alkorta, I.; Sánchez-Sanz, G.; Elguero, J.; Del Bene, J. E. Influence of hydrogen bonds on the P···P pnicogen bond. *J. Chem. Theory Comput.* **2012**, *8*, 2320−2327.
(52) Ma, N.; Zhang, Y.; Ji, B.; Tian, A.; Wang, W. Structural competition between halogen bonds and lone-pair..p interactions in solution. *ChemPhysChem* **2012**, *13*, 1411−1414.
(53) Jooneghani, S. G. N.; Gholipour, A. Mutual cooperation of π-π stacking and pnicogen bond interactions of substituted monomeric Lawesson's reagent and pyridine rings: Theoretical insight into Pyr||X-PhPS2⊥pyr complexes. *Chem. Phys. Lett.* **2019**, *721*, 91−98.
(54) Watson, B.; Grounds, O.; Borley, W.; Rosokha, S. V. Resolving the halogen vs. hydrogen bonding dichotomy in solutions: intermolecular complexes of trihalomethanes with halide and pseudohalide anions. *Phys. Chem. Chem. Phys.* **2018**, *20*, 21999−22007.
(55) Xu, Y.; Gabidullin, B.; Bryce, D. L. Single-Crystal NMR Characterization of Halogen Bonds. *J. Phys. Chem. A* **2019**, *123*, 6194−6209.
(56) Parra, R. D.; Grabowski, S. J. Enhancing Effects of the Cyano Group on the C-X···N Hydrogen or Halogen Bond in Complexes of X-Cyanomethanes with Trimethyl Amine: $CH_{3-}n(CN)_nX\cdots NMe_3$, (n = 0−3; X = H, Cl, Br, I). *Int. J. Mol. Sci.* **2022**, *23*, No. 11289.
(57) Scheiner, S. Ability of IR and NMR Spectral Data to Distinguish between a Tetrel Bond and a Hydrogen Bond. *J. Phys. Chem. A* **2018**, *122*, 7852−7862.
(58) Lu, J.; Scheiner, S. Effects of Halogen, Chalcogen, Pnicogen, and Tetrel Bonds on IR and NMR Spectra. *Molecules* **2019**, *24*, No. 2822.
(59) Michalczyk, M.; Zierkiewicz, W.; Wysokiński, R.; Scheiner, S. Theoretical Studies of IR and NMR Spectral Changes Induced by Sigma-Hole Hydrogen, Halogen, Chalcogen, Pnicogen, and Tetrel Bonds in a Model Protein Environment. *Molecules* **2019**, *24*, No. 3329.
(60) Lu, J.; Scheiner, S. Relationships between Bond Strength and Spectroscopic Quantities in H-Bonds and Related Halogen, Chalcogen, and Pnicogen Bonds. *J. Phys. Chem. A* **2020**, *124*, 7716−7725.
(61) Amonov, A.; Scheiner, S. Relation between Halogen Bond Strength and IR and NMR Spectroscopic Markers. *Molecules* **2023**, *28*, No. 7520.
(62) Attrell, R. J.; Widdifield, C. M.; Korobkov, I.; Bryce, D. L. Weak Halogen Bonding in Solid Haloanilinium Halides Probed Directly via Chlorine-35, Bromine-81, and Iodine-127 NMR Spectroscopy. *Cryst. Growth Des.* **2012**, *12*, 1641−1653.
(63) Latajka, Z.; Scheiner, S. Correlation between interaction energy and shift of the carbonyl stretching frequency. *Chem. Phys. Lett.* **1990**, *174*, 179−184.
(64) Bellamy, L. J.; Pace, R. J. Hydrogen bonding in alcohols and phenols. III. Hydrogen bonds between alcohols and carbonyl groups. *Spectrochim. Acta* **1971**, *27A*, 705−713.
(65) Thijs, R.; Zeegers-Huyskens, T. Infrared and Raman studies of hydrogen bonded complexes involving acetone, acetophenone and benzophenone I. Thermodynamic constants and frequency shifts of the n_{OH} and $n_{C=O}$ stretching vibrations. *Spectrochim. Acta, Part A* **1984**, *40*, 307−313.
(66) Bhattacharya, I.; Banerjee, P. From 'halogen' to 'tetrel' bonds: matrix isolation IR spectroscopic and quantum mechanical studies of the effect of central atom substitution in donor tetrahalogens on binary complex formation with formic acid. *Phys. Chem. Chem. Phys.* **2024**, *26*, 21538−21547.

https://doi.org/10.1021/acs.jpca.4c08283
J. Phys. Chem. A 2025, 129, 545−554

(67) Scheiner, S.; Michalczyk, M.; Zierkiewicz, W. Correlation between Noncovalent Bond Strength and Spectroscopic Perturbations within the Lewis Base. *J. Phys. Chem. A* **2024**, *128*, 10875−10883.
(68) Cogne, A.; Grand, A.; Laugier, J.; Robert, J. B.; Wiesenfeld, L. Anisotropy of the 1J(PSe) spin-spin coupling. X-ray and liquid crystal NMR study of trimethylphosphine selenide. *J. Am. Chem. Soc.* **1980**, *102*, 2238−2242.
(69) Viger-Gravel, J.; Meyer, J. E.; Korobkov, I.; Bryce, D. L. Probing halogen bonds with solid-state NMR spectroscopy: observation and interpretation of J(77Se,31P) coupling in halogen-bonded P═Se···I motifs. *CrystEngComm* **2014**, *16*, 7285−7297.
(70) Krutin, D. V.; Zakharov, A. S.; Tupikina, E. Y.; Mulloyarova, V. V. Unveiling the electronic structure peculiarities of phosphine selenides as NMR probes for non-covalent interactions: an experimental and theoretical study. *Phys. Chem. Chem. Phys.* **2024**, *26*, 20450−20461.
(71) Zakharov, A. S.; Krutin, D. V.; Mosalyov, P. O.; Tupikina, E. Y.; Antonov, A. S.; Tolstoy, P. M.; Mulloyarova, V. V. Phosphine selenides: versatile NMR probes for analyzing hydrogen OH···Se and halogen I···Se bonds. *Phys. Chem. Chem. Phys.* **2024**, *26*, 24488−24497.
(72) Frisch, M. J.; Trucks, G. W.; Schlegel, H. B.; Scuseria, G. E.; Robb, M. A.; Cheeseman, J. R.; Scalmani, G.; Barone, V.; Petersson, G. A.; Nakatsuji, H.et al. *Gaussian 16*; Rev. C.01; Gaussian Inc.: Wallingford, CT, 2016.
(73) Weigend, F. Accurate Coulomb-fitting basis sets for H to Rn. *Phys. Chem. Chem. Phys.* **2006**, *8*, 1057−1065.
(74) Zhao, Y.; Truhlar, D. G. Density functionals with broad applicability in chemistry. *Acc. Chem. Res.* **2008**, *41*, 157−167.
(75) Zhao, Y.; Truhlar, D. G. The M06 suite of density functionals for main group thermochemistry, thermochemical kinetics, noncovalent interactions, excited states, and transition elements: two new functionals and systematic testing of four M06-class functionals and 12 other functionals. *Theor. Chem. Acc.* **2008**, *120*, 215−241.
(76) Paytakov, G.; Dinadayalane, T.; Leszczynski, J. Toward Selection of Efficient Density Functionals for van der Waals Molecular Complexes: Comparative Study of C−H···π and N−H···π Interactions. *J. Phys. Chem. A* **2015**, *119*, 1190−1200.
(77) Vamhindi, B. S. D. R.; Karton, A. Can DFT and ab initio methods adequately describe binding energies in strongly interacting C_6X_6···C_2X_n π−π complexes? *Chem. Phys.* **2017**, *493*, 12−19.
(78) Podeszwa, R.; Szalewicz, K. Density functional theory overcomes the failure of predicting intermolecular interaction energies. *J. Chem. Phys.* **2012**, *136*, No. 161102.
(79) Karthikeyan, S.; Ramanathan, V.; Mishra, B. K. Influence of the substituents on the CH···p interaction: Benzene−methane complex. *J. Phys. Chem. A* **2013**, *117*, 6687−6694.
(80) Majumder, M.; Mishra, B. K.; Sathyamurthy, N. CH···p and p···p interaction in benzene-acetylene clusters. *Chem. Phys.* **2013**, *557*, 59−65.
(81) Vincent, M. A.; Hillier, I. H. The structure and interaction energies of the weak complexes of $CHClF_2$ and CHF_3 with HCCH: A test of denstiy functional theory methods. *Phys. Chem. Chem. Phys.* **2011**, *13*, 4388−4392.
(82) Boese, A. D. Density Functional Theory and Hydrogen Bonds: Are We There Yet? *ChemPhysChem* **2015**, *16*, 978−985.
(83) Walker, M.; Harvey, A. J. A.; Sen, A.; Dessent, C. E. H. Performance of M06, M06-2X, and M06-HF Density Functionals for Conformationally Flexible Anionic Clusters: M06 Functionals Perform Better than B3LYP for a Model System with Dispersion and Ionic Hydrogen-Bonding Interactions. *J. Phys. Chem. A* **2013**, *117*, 12590−12600.
(84) Molnar, L. F.; He, X.; Wang, B.; Merz, K. M. Further analysis and comparative study of intermolecular interactions using dimers from the S22 database. *J. Chem. Phys.* **2009**, *131*, No. 065102.
(85) Boys, S. F.; Bernardi, F. The calculation of small molecular interactions by the differences of separate total energies. Some procedures with reduced errors. *Mol. Phys.* **1970**, *19*, 553−566.
(86) Lu, T.; Chen, F. Quantitative analysis of molecular surface based on improved Marching Tetrahedra algorithm. *J. Mol. Graphics Modell.* **2012**, *38*, 314−323.
(87) Lu, T.; Chen, F. Multiwfn: A multifunctional wavefunction analyzer. *J. Comput. Chem.* **2012**, *33*, 580−592.
(88) Humphrey, W.; Dalke, A.; Schulten, K. VMD: Visual molecular dynamics. *J. Mol. Graphics* **1996**, *14*, 33−38.
(89) Bader, R. F. W. A Bond Path: A Universal Indicator of Bonded Interactions. *J. Phys. Chem. A* **1998**, *102*, 7314−7323.
(90) Popelier, P. L. A. *Atoms in Molecules. An Introduction.*; Prentice Hall: Harlow, UK, 2000.
(91) Keith, T. A. *AIMAll*; TK Gristmill Software: Overland Park KS, 2013.
(92) Horn, P. R.; Mao, Y.; Head-Gordon, M. Probing non-covalent interactions with a second generation energy decomposition analysis using absolutely localized molecular orbitals. *Phys. Chem. Chem. Phys.* **2016**, *18*, 23067−23079.
(93) Horn, P. R.; Mao, Y.; Head-Gordon, M. Defining the contributions of permanent electrostatics, Pauli repulsion, and dispersion in density functional theory calculations of intermolecular interaction energies. *J. Chem. Phys.* **2016**, *144*, No. 114107.
(94) Espinosa, E.; Molins, E.; Lecomte, C. Hydrogen bond strengths revealed by topological analyses of experimentally observed electron densities. *Chem. Phys. Lett.* **1998**, *285*, 170−173.
(95) Espinosa, E.; Alkorta, I.; Rozas, I.; Elguero, J.; Molins, E. About the evaluation of the local kinetic, potential and total energy densities in closed-shell interactions. *Chem. Phys. Lett.* **2001**, *336*, 457−461.
(96) Mata, I.; Alkorta, I.; Espinosa, E.; Molins, E. Relationships between interaction energy, intermolecular distance and electron density properties in hydrogen bonded complexes under external electric fields. *Chem. Phys. Lett.* **2011**, *507*, 185−189.

https://doi.org/10.1021/acs.jpca.4c08283
J. Phys. Chem. A 2025, 129, 545−554